Chemical Science

RSC Publishing

EDGE ARTICLE

View Article Online
View Journal | View Issue

Cite this: *Chem. Sci.*, 2013, **4**, 1189

Uncovering f-element bonding differences and electronic structure in a series of 1 : 3 and 1 : 4 complexes with a diselenophosphinate ligand†

Matthew B. Jones,[a] Andrew J. Gaunt,*[a] John C. Gordon,[a] Nikolas Kaltsoyannis,*[b] Mary P. Neu[c] and Brian L. Scott[d]

Understanding the bonding trends within, and the differences between, the 4f and 5f element series with soft donor atom ligands will aid elucidation of the fundamental origins of actinide (An) *versus* lanthanide (Ln) selectivity that is integral to many advanced nuclear fuel cycle separation concepts. One of the principal obstacles to acquiring such knowledge is the dearth of well characterized transuranic molecules that prevents the necessary comparison of 4f *versus* 5f coordination chemistry, electronic structure, and bonding. Reported herein is new chemistry of selenium analogues of dithiophosphinate actinide extractants. Ln^{III} and $An^{III/IV}$ complexes with the diselenophosphinate $[Se_2PPh_2]^-$ anion have been synthesized, structurally and spectroscopically characterized, and quantum chemical calculations performed on model compounds in which the phenyl rings have been replaced by methyl groups. The complexes $[Ln^{III}(Se_2PPh_2)_3(THF)_2]$ (Ln = La (**1**), Ce (**2**), Nd (**3**)), $[La^{III}(Se_2PPh_2)_3(MeCN)_2]$ (**4**), $[Pu^{III}(Se_2PPh_2)_3(THF)_2]$ (**5**), $[Et_4N][M^{III}(Se_2PPh_2)_4]$ (M = Ce (**6**), Pu (**7**)), and $[An^{IV}(Se_2PPh_2)_4]$ (An = U (**8**), Np (**9**)), represent the first f-element diselenophosphinates. In conjunction with the calculated models, complexes **1–9** were utilized to examine two important factors: firstly, bonding trends/differences between trivalent 4f and 5f cations of near identical ionic radii; secondly, bonding trend differences across the 5f series within the An^{IV} oxidation state. Analysis of both experimental and computational data supports the conclusion of enhanced covalent bonding contributions in Pu^{III}–Se *versus* Ce^{III}–Se bonding, while differences between U^{IV}–Se and Np^{IV}–Se bonding is satisfactorily accounted for by changes in the strength of ionic interactions as a result of the increased positive charge density on Np^{IV} compared to U^{IV} ions. These findings improve understanding of soft donor ligand binding to the f-elements, and are of relevance to the design and manipulation of f-element extraction processes.

Received 22nd October 2012
Accepted 23rd November 2012

DOI: 10.1039/c2sc21806b

www.rsc.org/chemicalscience

Introduction

A detailed understanding of actinide coordination chemistry is of intrinsic value to advanced nuclear fuel cycle topics, such as spent fuel separations, nuclear waste remediation, and environmental speciation/mobility.[1–4] Some of the most difficult separation challenges and environmental concerns pertain to transuranic radioisotopes, which are the least studied of the f-elements. The paucity of examples of transuranic coordination compounds in the literature, therefore, represents a major knowledge gap to be addressed. The lack of reported complexes of these elements also hinders progress to an acceptable level of understanding of the actinide series as a whole; for example, how the chemistry changes with varying oxidation states, and how 5f metal chemistry compares to that of the lanthanides.

One highly debated topic is the degree to which covalency plays a role in An^{III}/Ln^{III} separations.[5–11] Selective separation of these sets of trivalent cations is very difficult because of their close chemical properties and similar binding strength to traditional hard oxygen donor extractant molecules. However, certain ligands containing "soft" donor atoms, such as N or S, have been shown to display a high affinity for binding An^{III} over similarly sized Ln^{III} ions. An exceptional example of this is the organodithiophosphinate ($R_2PS_2^-$) class of ligands, some of which display the largest An^{III}/Ln^{III} separation factors observed to date.[12–14] However, the determination of the precise electronic factors that govern this selectivity, and the extent to which differential covalency is important, has proven elusive.

[a]*Chemistry Division, Los Alamos National Laboratory, Los Alamos, New Mexico 87545, USA. E-mail: gaunt@lanl.gov*

[b]*Department of Chemistry, University College London, 20 Gordon Street, London, WC1H 0AJ, UK. E-mail: n.kaltsoyannis@ucl.ac.uk*

[c]*Weapons Program, Los Alamos National Laboratory, Los Alamos, New Mexico 87545, USA*

[d]*Materials Physics and Applications Division, Los Alamos National Laboratory, Los Alamos, New Mexico 87545, USA*

† Electronic supplementary information (ESI) available. CCDC 906766–906774. For ESI and crystallographic data in CIF or other electronic format see DOI: 10.1039/c2sc21806b

One strategy that has been used to probe the degree of covalency within f-element complexes featuring soft donor ligands has been to compare metrical data from the crystal structures of isostructural complexes of 4f and 5f ions of similar ionic radii.[5,8,15–17] Differences in M–L bond lengths have been utilized as a parameter for the degree of covalency, with statistically significant shorter bonds usually (there are exceptions) being related to stronger, more covalent bonds. There are, however, some drawbacks to this strategy which should be kept in mind when studying f-element soft donor bonding with this approach.[18] Factors such as crystal packing forces can have an influence over variability in bond length, particularly as the bonds can have rather flat potential surfaces in the equilibrium region, making comparisons of structures in different crystal systems complicated. Also, useful separation factors can be achieved through relatively small energetic differences (*ca.* 3 kcal mol^{-1}), which render detection *via* statistically significant bond length changes very difficult.

Computational methods have also been employed in order to provide a rationale for the observed separation factors, and in particular for the subtle bond length differences observed experimentally.[5,19–26] Central to these studies is the quantum chemical assessment of covalency in the f-element–ligand bond,[27–30] but this is by no means a straightforward exercise, as discussed at some length previously.[31] More specifically, the energetic proximity of actinide valence 5f and ligand orbitals can result in MOs with significant contributions from both atoms, yet little spatial overlap, yielding highly mixed orbitals but no significant internuclear build-up of electron density. In such circumstances it is questionable that the more traditional quantum chemical measures of covalency such as MO compositions and atomic spin densities yield unambiguous results, and additional approaches may be required.

Some of the complicating factors in drawing bond length comparisons can be mitigated, to some extent, by a well crafted study and judicious choice of ligand system. Isostructural homoleptic complexes with only one type of bond in the inner metal coordination sphere allow easier analysis than complexes containing multiple bond types, multiple donor atom types, hydrogen bonding effects, or those that are isolated in different crystal systems/space groups. Furthermore, when possible, comparison of individual bond distances between isostructural systems can be more insightful than taking average values, which will often have a large associated standard deviation value. In order to attempt to emphasise 4f *versus* 5f covalency differences, and render them more readily observable experimentally and computationally, it is logical to employ 'very soft' models of extractant molecules, *e.g.* to introduce Se or Te donor atoms in place of S donor atoms. Davies and co-workers previously reported the synthesis of the diphenyldiselenophosphinate ligand, $[K(Se_2PPh_2)]_2$, a selenium analogue of dithiophosphinate extractant molecules.[32] While no f-block complexes of this ligand have been reported to date, it is well suited to test the hypothesis that An^{III} ions have greater covalency in their bonding with soft donor ligands than Ln^{III} ions of similar ionic radii. Thus, in this contribution, we provide the first experimental and theoretical comparison of structurally similar $[Se_2PPh_2]^-$ complexes of trivalent An and Ln ions, as well as making a comparison between two different An^{IV} complexes, containing U^{IV} and Np^{IV}.

Results and discussion

Trivalent 1 : 3 complexes

Heating the diselenophosphinate dimer $[K(Se_2PPh_2)]_2$ with 0.66 equivalents of LnX_3 (LnX_3 = $La(OTf)_3$, $CeBr_3$, or $NdCl_3$) in THF results in the formation of neutral complexes with formula $[Ln(Se_2PPh_2)_3(THF)_2]$ (Ln = La (**1**), Ce (**2**), Nd (**3**)) (Scheme 1).

The molecular structures of **1–3** feature eight-coordinate metal centers with three $[Se_2PPh_2]^-$ ligands bound through both Se atoms as well as two coordinated THF solvent molecules. Compounds **1** and **3** are isostructural in a tetragonal crystal system and $P4_2/nmc$ space group, whereas **2** crystallized in a triclinic crystal system in the $P\bar{1}$ space group. The three $[Se_2PPh_2]^-$ ligands are bound in a pseudo-equatorial arrangement around the metal center, with the THF ligands occupying the axial positions (Fig. 1). In **1** and **3**, two of the three $[Se_2PPh_2]^-$ ligands have the three 'SePSe' atoms of the diselenophosphinate moiety in a nearly co-planar arrangement.

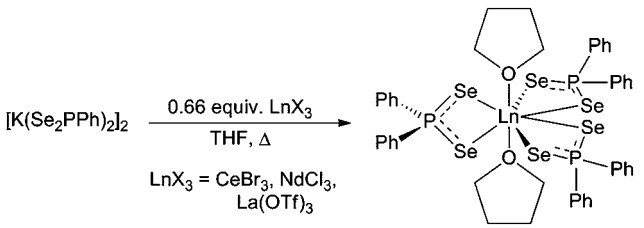

Scheme 1 Synthesis of 1 : 3 metal–ligand, $[Ln(Se_2PPh_2)_3(THF)_2]$ (Ln = La (**1**), Ce (**2**), Nd (**3**)), complexes.

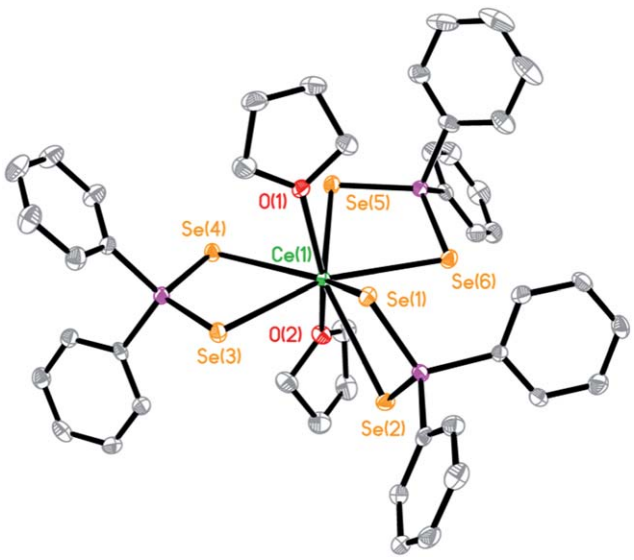

Fig. 1 Solid-state structure of $[Ce(Se_2PPh_2)_3(THF)_2]$ (**2**). Hydrogen atoms are omitted for clarity. Thermal ellipsoids are shown at the 50% probability level. The La (**1**) and Nd (**3**) complexes contain identical molecular connectivity as **2** but occupy a different crystal system and space group.

The 'SePSe' moiety of the third ligand is perpendicular to the others, lying in the same plane as the oxygen atoms of the THF ligands. In complex **2**, the ligands are positioned in same basic arrangement as in **1** and **3**, except that **2** has lower symmetry and the 'SePSe' moieties are significantly bent away from the co-planarity described for **1** and **3**. For all three complexes, the geometry around the lanthanide ion is best described as a distorted dodecahedron, according to the criteria laid out by Haigh,[33] with the distortion being greater in **2** than in **1** or **3** (the gap between the 16th and 17th lowest ligand–metal–ligand angles is about 14° in **2**, but only about 7.5° in **1** and **3**). The M–O and M–Se bond distances for **1–3** are shown in Table 1. Table 1 also presents metal–ligand bond lengths obtained from DFT calculations carried out on models for **1–3**, in which the phenyl rings were replaced by methyl groups. These compounds are labelled **1a**, **2a**, and **3a**. Agreement between theory and experiment is generally very good for the M–Se bonds, with a mean absolute deviation of the average Me–Se bond length of just 0.023 Å. The M–O bond distances are reproduced less well by the calculations.

Moving from left to right across the lanthanide series, the expectation is that metal–ligand bond distances will decrease for bonds dominated by ionic interactions due to the greater charge density of the Ln^{3+} ions. Comparing the experimentally derived longest and shortest Ln–Se bonds, the Ce–Se bonds in **2** are actually slightly longer than the corresponding La–Se bonds in **1**. However, there is a large distance range between the longest and shortest M–Se bonds and, as a result, attempting to draw any statistically significant conclusions about bond length differences between **1** and **2** from comparison of average Ln–Se bond lengths is not possible given the large standard deviation associated with those values. Continuing right across the 4f series from Ce to Nd, comparison of the longest and shortest Ln–Se bonds with each other is consistent with an expected shortening from Ce–Se bonds in **2** to Nd–Se bonds in **3**; however, again the large spread of values prevents meaningful conclusions to be drawn upon comparison of average Ln–Se distances. The calculated data are a little clearer, however, with a *ca.* 0.05 Å decrease in the M–Se distances from **1a** to **3a**, consistent with the reduction in the eight-coordinate Ln^{III} ionic radii from La^{3+} (1.160 Å) to Nd^{3+} (1.109 Å).[34]

For Ln = La, the MeCN adduct $[La(Se_2PPh_2)_3(MeCN)_2]$ (**4**) was also prepared by changing the reaction medium from THF to acetonitrile. X-ray quality crystals of **4** were obtained by diffusion of diethyl ether into a concentrated acetonitrile solution of $[La(Se_2PPh_2)_3(MeCN)_2]$. The structure reveals identical molecular connectivity to **1** but with MeCN ligands in place of THF (Fig. 2). There are no significant differences in the average La–Se bond lengths between **1** and **4** (see Table 1; note that attempts to converge the geometry of a computational model for **4** proved unsuccessful). However, in **4** none of the 'SePSe' groups of the

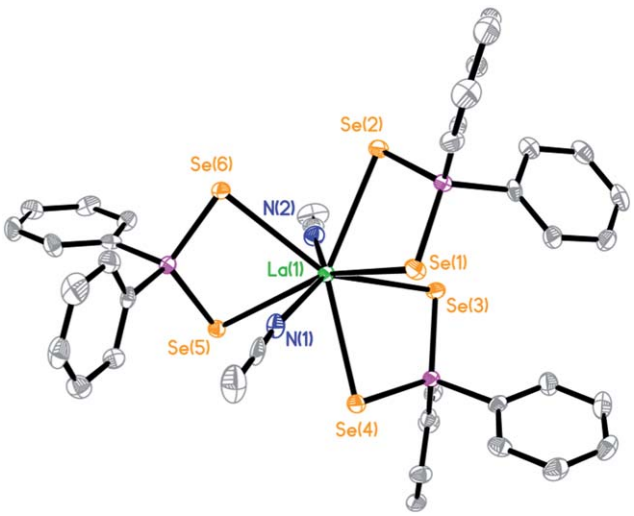

Fig. 2 Solid-state structure of $[La(Se_2PPh_2)_3(MeCN)_2]$ (**4**). Hydrogen atoms are omitted for clarity. Thermal ellipsoids are shown at the 50% probability level.

Table 1 Selected experimental bond distances (Å) for $[Ln(Se_2PPh_2)_3(Sol)_2]$ (Sol = THF, MeCN) complexes (**1–4**), and calculated data for model compounds **1a–3a** in italics. To aid metrical comparison, the values are numbered and listed in order of decreasing length from top to bottom for each bond type, and are not listed by atom labelling schemes in the crystallographic files

Bond	$[La(Se_2PPh_2)_3(THF)_2]$ (**1**/**1a**)	$[Ce(Se_2PPh_2)_3(THF)_2]$ (**2**/**2a**)	$[Nd(Se_2PPh_2)_3(THF)_2]$ (**3**/**3a**)	$[La(Se_2PPh_2)_3(MeCN)_2]$ (**4**)
M–Se_1	3.1483(15)	3.1892(5)	3.1120(7)	3.1121(5)
	3.173	*3.154*	*3.132*	
M–Se_2	3.1444(15)	3.1285(5)	3.1054(8)	3.1081(5)
	3.171	*3.148*	*3.123*	
M–Se_3	3.1072(11)	3.1068(5)	3.0601(5)	3.1021(5)
	3.154	*3.135*	*3.102*	
M–Se_4	3.0750(9)	3.0973(5)	3.0218(5)	3.0943(5)
	3.132	*3.105*	*3.088*	
M–Se_5	Symmetry generated	3.0867(5)	Symmetry generated	3.0736(6)
	3.130	*3.095*	*3.085*	
M–Se_6	Symmetry generated	3.0674(5)	Symmetry generated	3.0689(5)
	3.106	*3.065*	*3.041*	
M–Sol_1	2.575(8)	2.496(2)	2.530(4)	2.689(4)
	2.620	*2.622*	*2.574*	
M–Sol_2	2.502(8)	2.479(2)	2.452(4)	2.630(4)
	2.596	*2.589*	*2.536*	

$[Se_2PPh_2]^-$ ligands are close to co-planar, and are all twisted with respect to each other. This subtle geometric change could be due to the decreased steric demands of acetonitrile compared to THF. The geometry about the lanthanum ion is best described as distorted square antiprismatic, according to Haigh's criteria, with the difference between the 16th and 17th lowest ligand–metal–ligand angles being 26.39°.

^{31}P NMR spectra of the diamagnetic La^{III} complexes **1** and **4**, in $CDCl_3$, display a single resonance (Table 2), indicating that the subtle differences in ligand arrangement noticeable in the solid state are not reflected by any ^{31}P NMR chemical shift differences in solution. Complexes **2** and **3** exhibit ^{31}P NMR resonances with large chemical shifts, as expected due to the paramagnetic nature of Ce^{III} and Nd^{III} ions.

With lanthanide complexes in hand, we sought to synthesize and isolate a Pu^{III} complex for comparison. The small milligram scales and practicalities of working with the high specific-activity ^{239}Pu radionuclide introduce some synthetic nuances and limitations, details of which are discussed elsewhere.[2,35,36] These considerations resulted in our synthetic efforts focusing solely upon using $[PuI_3(py)_4]$ as the Pu^{III}-containing starting material, rather than exploring the reaction chemistry of multiple Pu^{III} synthetic precursors. Addition of 1.5 equivalents of $[K(Se_2PPh_2)]_2$ to a pyridine solution of $[PuI_3(py)_4]$ followed by heating for 45 minutes afforded a green solid that we postulate as $[Pu(Se_2PPh_2)_3(py)_2]$ based upon ^{1}H and ^{31}P NMR data as well as knowledge of the lanthanide chemistry learned during the syntheses of **1–4**. Attempts to grow X-ray quality crystals of the putative "$[Pu(Se_2PPh_2)_3(py)_2]$" product proved unfruitful. Changing the reaction medium from pyridine to THF yielded a green solid product that appeared by ^{1}H NMR spectroscopy to be a mixture of the pyridine adduct and the THF solvento adduct $[Pu(Se_2PPh_2)_3(THF)_2]$. Analysis of this mixture by ^{31}P NMR showed only one resonance (−184 ppm), presumably due to frequency overlap as a result of the close similarity of the pyridine and THF solvento complexes. Attempts to displace all of the coordinated pyridine molecules and quantitatively drive the reaction to the THF adduct were unsuccessful (at most, 75% of the crude product was determined to be the THF adduct by integration of the ^{1}H NMR spectrum). However, X-ray diffraction quality crystals of $[Pu(Se_2PPh_2)_3(THF)_2]$ (**5**) could be grown, albeit in very low yield, by diffusion of hexanes into a 1 : 1 THF–toluene solution of the product. Compound **5** contains the same molecular connectivity as the lanthanide complexes **1–3**. Three bidentate $[Se_2PPh_2]^-$ ligands are in a pseudo-equatorial arrangement around the metal center, and the THF ligands occupy the axial positions (Fig. 3). The arrangement of the 'SePSe' groups of the ligands with respect to each other is essentially identical to that in **1** and **3** rather than the more bent/twisted arrangement that exists in **2**. The unit cell of **5** features two crystallographically independent $[Pu(Se_2PPh_2)_3(THF)_2]$ molecules. The two independent eight-coordinate Pu^{III} centers are both probably best described as occupying a distorted docdecahedral geometry according to Haigh's criteria (with the distortion for Pu(1) towards a bicapped trigonal prism as evidenced by a gap between the 17th and 18th lowest ligand–metal–ligand angles of 10.27°, whereas there is no substantial gap between the corresponding angles for Pu(2)). Crystallographic information is listed in Table 6, and selected metrical parameters for each unique molecule are given in Table 3, together with metal–ligand bond lengths obtained from DFT calculation of model compound **5a**.

As discussed in the Introduction, in certain cases, bond length comparisons between An^{III} and Ln^{III} ions can be an indicator of differences that are not satisfactorily explained by ionic bonding contributions alone. In the case of Pu^{III}, we have chosen the best 4f metal comparison to examine for these differences as Ce^{III} because of its similar ionic radius to Pu^{III}. The ionic radii reported by Shannon for six-coordinate Pu^{III} and Ce^{III} are 1.00 and 1.01 Å, respectively.[34] The ionic radius for eight-coordinate Pu^{III} is not available in ref. 34 but we note that in the tetravalent case for these metals, the ionic radius of Ce(IV) increases 0.10 Å from six- to eight-coordination, while the corresponding increase for Pu(IV) is also 0.10 Å. The determination of the ionic radii were based primarily upon 'hard' binary oxide and fluoride compounds, with the aim of mitigating any effects of multiple types of bonding modes, hydrogen bonding, multiple ligand types, solvent inclusion, *etc.* During the

Table 2 ^{31}P NMR resonances for compounds in **1–9** dissolved in deuterated solvent

Complex	^{31}P Shift (ppm)
$[La(Se_2PPh_2)_3(THF)_2]$	17
$[Ce(Se_2PPh_2)_3(THF)_2]$	−58
$[Nd(Se_2PPh_2)_3(THF)_2]$	−278
$[La(Se_2PPh_2)_3(MeCN)_2]$	17
$[Pu(Se_2PPh_2)_3(THF)_2]$	−184
$[Et_4N][Ce(Se_2PPh_2)_4]$	−68
$[Et_4N][Pu(Se_2PPh_2)_4]$	−170
$[U(Se_2PPh_2)_4]$	−810
$[Np(Se_2PPh_2)_4]$	−902

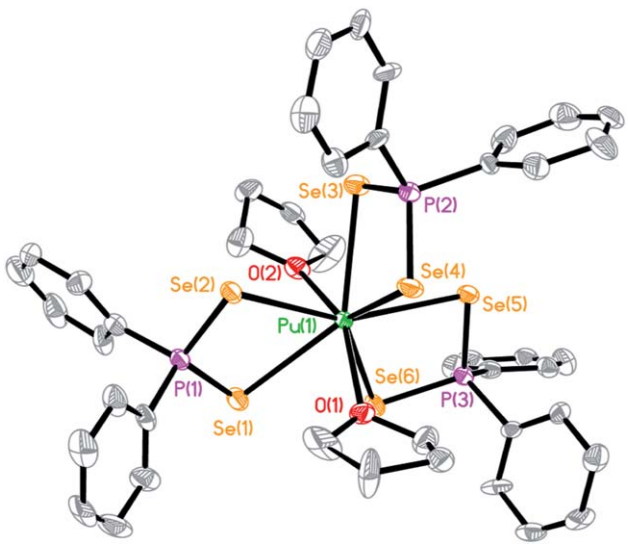

Fig. 3 Solid-state structure of $[Pu(Se_2PPh_2)_3(THF)_2]$ (**5**). Hydrogen atoms are omitted for clarity. Thermal ellipsoids are shown at the 50% probability level. Only one of the two crystallographically independent molecules is shown.

Table 3 Selected experimental bond distances (Å), for $[Ce(Se_2PPh_2)_3(THF)_2]$ (**2**) and $[Pu(Se_2PPh_2)_3(THF)_2]$ (**5**), and calculated data for model compounds **2a** and **5a** in italics[a]

Bond	$[Ce(Se_2PPh_2)_3(THF)_2]$ (**2**/*2a*)	$[Pu(Se_2PPh_2)_3(THF)_2]$ Pu(1)	$[Pu(Se_2PPh_2)_3(THF)_2]$ Pu(2) (**5**/*5a*)	Δ for Ce–Pu(1), Ce–Pu(2), and *Δ for M–Se* (**2a**/*5a*)
$M–Se_1$	3.1892(5)	3.1128(14)	3.1323(15)	0.0764, 0.0569
	3.154		*3.140*	*0.014*
$M–Se_2$	3.1285(5)	3.0989(14)	3.1138(14)	0.0296, 0.0147
	3.148		*3.128*	*0.020*
$M–Se_3$	3.1068(5)	3.0667(15)	3.0879(15)	0.0401, 0.0189
	3.135		*3.103*	*0.032*
$M–Se_4$	3.0973(5)	3.0663(13)	3.0723(14)	0.0310, 0.0250
	3.105		*3.093*	*0.012*
$M–Se_5$	3.0867(5)	3.0414(14)	3.0719(14)	0.0454, 0.0148
	3.095		*3.064*	*0.031*
$M–Se_6$	3.0674(5)	3.0354(13)	3.0627(13)	0.0320, 0.0113
	3.065		*3.037*	*0.028*
$M–O_1$	2.496(2)	2.516(8)	2.502(8)	−0.020, −0.006
	2.622		*2.551*	*0.071*
$M–O_2$	2.479(2)	2.510(8)	2.466(7)	−0.031, 0.013
	2.589		*2.536*	*0.053*

[a] Avg Δ M–Se: 0.0424, 0.0236, *0.023*.

preparation of this manuscript, Albrecht-Schmitt and co-workers reported a redetermination of the ionic radius of eight-coordinate Pu^{III} from a heteroleptic, solvated phosphite compound.[37] Their analysis suggests that Nd^{III} is a better analog for Pu^{III}; however, because Shannon's values are based on simple compound types and are presented for many f-elements and oxidation states we have still chosen Ce as the best comparison to Pu, and we have not yet adopted the proposed new radius. As more isostructural transuranic/lanthanide compounds are isolated and characterized it will become clearer which lanthanides are the most accurate models for certain actinides and comparison studies will need to account for such new data accordingly.

The M–Se and M–O bond lengths in **2** and **5** are tabulated in Table 3. Since there are two unique molecules in the unit cell of **5**, we have chosen to compare each one separately to the Ce–Se distances in **2**. Table 3 organizes the M–Se bonds from longest to shortest, and taking each into consideration separately. Interestingly, every Ce–Se bond is found to be longer than each corresponding Pu–Se bond, which is the trend that would be expected for enhanced Pu–Se *versus* Ce–Se covalent bonding. However, the presence of two Pu molecules in each unit cell and the relatively large esd values associated with the Pu–Se distances makes drawing direct bond-to-bond comparisons very difficult, and the large range of M–Se distances in the Ce and Pu 1 : 3 complexes precludes statistically meaningful comparison of average values. Therefore, whilst the experimentally determined metrical data for the 1 : 3 complexes certainly do not contradict the hypothesis of increased covalency in the actinide bonding, neither can they provide conclusive support. However, that being stated, the calculated data for **2a** and **5a** reinforce the tentative experimental conclusions, with a consistent reduction in M–Se bond lengths of between 0.012 and 0.032 Å from Ce to Pu.

Besides the focus on comparison of metrical data, **1–5** represent the first examples of any lanthanide or actinide complexes with diselenophosphinate ligands, while only one class of any Se donor ligand coordinated to plutonium has previously been reported (imidodiphosphinochalcogenolates, which are not structurally related to actinide separation agents, in contrast to the $[Se_2PPh_2]^-$ anion of more separation relevance in the present study).[5] In addition, there are no reported examples of trivalent actinide complexes with analogous S donor dithiophosphinate ligands, preventing any comparison of the Pu–Se distances to An–S distances. For comparison to the only other examples of molecular plutonium–selenium bonds, the average Pu–Se distance in the imidodiphosphinoselenolate complex $Pu^{III}[N(SeP^iPr_2)_2]_3$ is 2.917 Å, in which the $[N(SeP^iPr_2)_2]^-$ ligand is bidentate, whilst in the $Pu^{III}[N(SePPh_2)_2]_3$ complex containing tridentate ligands (two Se donor atoms and one N donor atom), there is a single unique Pu–Se distance of 3.0710(2) Å.[5]

Homoleptic trivalent 1 : 4 anionic complexes

Given the complexities of drawing direct or conclusive bonding comparisons within the 1 : 3 series of complexes, we then attempted to isolate molecules that would be ideal for a Pu–Se *versus* Ce–Se bonding comparison. We sought to synthesize homoleptic 1 : 4 metal–ligand complexes with the $[Se_2PPh_2]^-$ anion (containing only M–Se bonds in the inner coordination sphere of the metal ion), in the hope that Pu^{III} and Ce^{III} compounds would crystallize in an identical unit cell/space group, contain low errors associated with the metrical data, and contain only one independent molecule per unit cell, thus allowing a direct and relatively simple Pu–Se *versus* Ce–Se bonding comparison. Gratifyingly, treatment of an acetonitrile solution of either $CeBr_3$ or $[PuI_3(py)_4]$ with two equivalents of $[K(Se_2PPh_2)]_2$ in the presence of Et_4NBr generates the complexes $[Et_4N][Ce(Se_2PPh_2)_4]$ (**6**) and $[Et_4N][Pu(Se_2PPh_2)_4]$ (**7**) (Schemes 2 and 3).

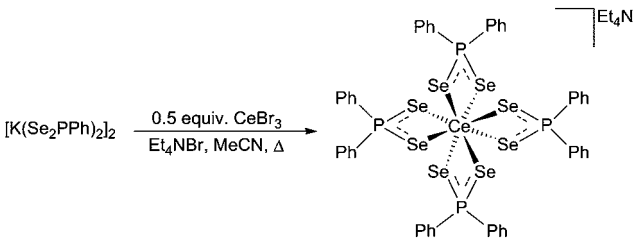

Scheme 2 Synthesis of the 1 : 4 metal–ligand Ce^{III} complex $[Et_4N][Ce(Se_2PPh_2)_4]$ (**6**).

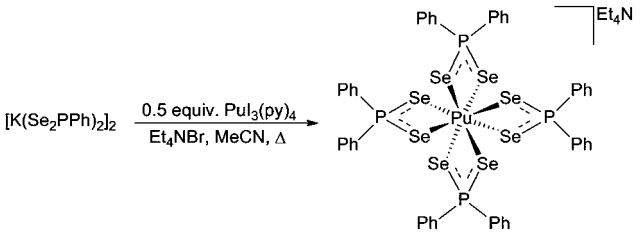

Scheme 3 Synthesis of the 1 : 4 metal–ligand Pu^{III} complex $[Et_4N][Pu(Se_2PPh_2)_4]$ (**7**).

The ^{31}P NMR spectra of $[Et_4N][Ce(Se_2PPh_2)_4]$ and $[Et_4N][Pu(Se_2PPh_2)_4]$ each display a paramagnetically shifted single resonance at −68 and −170 ppm, respectively (Table 2), and are distinct from the resonances for the corresponding 1 : 3 complexes, **2** and **5**. X-ray diffraction quality crystals of **6** and **7** were grown by diffusion of diethyl ether into a concentrated THF or THF/MeCN solution of the complexes. The solid-state crystal structures reveal that the complexes are isostructural, with four $[Se_2PPh_2]^-$ ligands each bound to the metal through both Se atoms (Fig. 4). The eight-coordinate Ce^{III} and Pu^{III} centers are probably best described as occupying a distorted docdecahedral geometry according to Haigh's criteria (with the distortion towards bicapped trigonal prisms as evidenced by gaps between the 17th and 18th lowest ligand–metal–ligand angles of 12.50° in **6** and 11.87° in **7**). Selected crystallographic data are presented in Table 6, and M–Se bond distances for the complexes are listed in Table 4. Both complexes crystallize in the $P2_12_12_1$ space group, and each structure also contains one lattice THF molecule per complex.

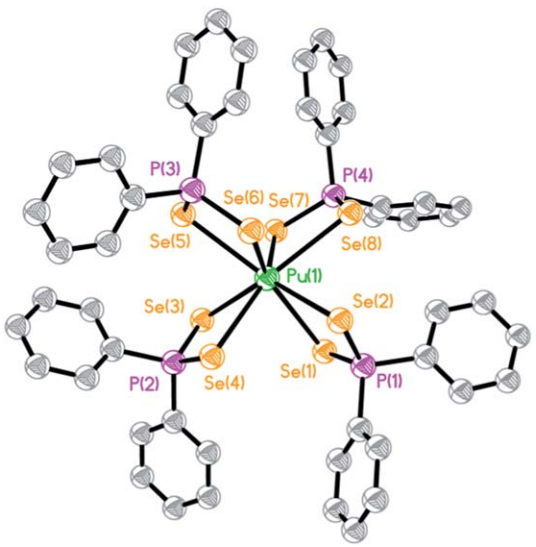

Fig. 4 Solid-state structure of $[Et_4N][Pu(Se_2PPh_2)_4]$ (**7**). The $[Et_4N]^+$ cation, lattice THF solvent, and hydrogen atoms are omitted for clarity. Thermal ellipsoids are shown at the 50% probability level. The Ce^{III} analogue, **6**, is isostructural.

Because of their similarities, the structures of these homoleptic complexes are ideal for comparison. Each of the eight M–Se bonds in **6** and **7** is unique. The complexes each have a distinct set of four long and four short M–Se bonds (one long and one short bond per individual ligand). The M–Se distances between **6** and **7** can be compared in a meaningful manner because the complexes are isostructural with excellent final R_1 values of 0.0269 and 0.0261, respectively. In Table 4, the M–Se bonds have been arranged into the two sets of long and short bonds and the atom numbering from **6** to **7** is directly mapped between the two structures, with the Se atom numbers corresponding to the numbering system in the crystallographic files. Thus, comparing each corresponding pair of M–Se bonds (same Se atom numbers in the crystallographic files of **6** and **7**), we find that the Pu–Se bond is significantly shorter than the Ce–Se bond in every case, suggesting that the bonding differences between these two isostructural complexes are not adequately explained by an ionic bonding model alone. The bond length differences are noticeably pronounced between the four shortest pairs, where Δ values are between 0.0414–0.0448 Å. Overall, the average difference in the Pu–Se *versus* Ce–Se bond length is 0.0297 Å. It would therefore seem reasonable to conclude that **6** and **7** provide metrical data that support a view of a modest enhancement of covalent contributions in the Pu–Se *versus* Ce–Se bonding. Unfortunately, computational attempts to converge the geometry of a methyl-based model for **7** proved unsuccessful, and so no direct comparison of theory with experiment is possible here. However, the present experimentally determined 0.0297 Å average bond length difference between Pu–Se and Ce–Se is rather similar to the 0.023 Å found computationally for the trivalent 1 : 3 complexes (Table 3).

Given that the theory of enhanced covalency in An^{III} soft donor complexes is proposed to lead to shorter An–ligand *versus* Ln–ligand bond distances, then, conversely, it might be expected that for molecules containing only 'hard' ionic bonds (for example, certain anionic oxygen donor ligands) to the metal the Pu^{III}–ligand *versus* Ce^{III}–ligand distances would be equal. This

Table 4 Selected bond distances (Å), for $[Et_4N][Ce(Se_2PPh_2)_4]$ (**6**) and $[Et_4N][Pu(Se_2PPh_2)_4]$ (**7**)[a]

Bond	$[Et_4N][Ce(Se_2PPh_2)_4]$	$[Et_4N][Pu(Se_2PPh_2)_4]$	Δ
M–Se(1)	3.0736(5)	3.0288(4)	0.0448
M–Se(4)	3.0229(5)	2.9815(4)	0.0414
M–Se(5)	3.0573(5)	3.0138(4)	0.0435
M–Se(8)	3.0409(5)	2.9990(4)	0.0419
M–Se(2)	3.1269(5)	3.1160(5)	0.0109
M–Se(3)	3.1190(5)	3.1058(4)	0.0132
M–Se(6)	3.1164(5)	3.0945(4)	0.0219
M–Se(7)	3.1251(5)	3.1050(4)	0.0201

[a] Avg Δ, M–Se: 0.0297.

postulation is difficult to demonstrate conclusively by a literature search, again largely due to the lack of structurally characterized homoleptic transuranic molecules from which to draw comparisons to lanthanide analogues. One recent example of isostructural Ce^{III} and Pu^{III} phosphonates (heteroleptic systems that form three-dimensional extended lattices) appeared, at first glance, to show shorter Pu–O *versus* Ce–O distances by an approximate magnitude of 0.022 Å; however, these differences are essentially identical within the 3σ criterion of statistical significance.[38] A similar bond length scenario was encountered in the recently reported isostructural phosphite system.[37] In complexes **6** and **7**, the esd values associated with the individual Ce–Se and Pu–Se bond lengths are an order of magnitude less than those in the reported phosphonate and phosphite systems, conferring confidence that the differences between **6** and **7** are statistically important. The phosphonate system also had the added complication that computational models implicated some occupancy of actinide d orbitals which may mean that these compounds are not suitable benchmark examples to examine for differences in 'ionic-only' Ce–O and Pu–O bonding comparisons. No computational analyses were presented for the phosphite systems in ref. 37. Nonetheless, there is clear potential benefit of more studies with the aim of comparisons between Ce–O *versus* Pu–O distances (with low associated esd values) in homoleptic isostructural molecular systems being drawn to more accurately determine if indeed Ce–O *versus* Pu–O distances are generally equal in 'ionic-only' bonds (and, in turn, inform upon the accuracy of Ce^{III} as the best analogue for Pu^{III} in terms of ionic radius).

Tetravalent actinide 1 : 4 complexes

In addition to trivalent complexes, homoleptic 1 : 4 An^{IV} complexes with the $[Se_2PPh_2]^-$ ligand have been structurally characterized. Addition of two equivalents of $[K(Se_2PPh_2)]_2$ to a THF solution of $[UI_3(THF)_4]$ unintentionally afforded the neutral complex $[U(Se_2PPh_2)_4]$ (**8**) after 24 hours of stirring. While oxidation of U^{III} to U^{IV} was not intended, it has been observed before in situations where it is not obvious what entity is acting as the oxidant.[39] Consequently, the isolated yield of pure **8** was very low and we were not able to fully characterize the product, although a single, paramagnetically shifted, ^{31}P NMR resonance at −810 ppm in C_6D_6 solution was observed and attributed to **8**. The single-crystal X-ray structure was also obtained. Subsequently, the Np(IV) analog, $[Np(Se_2PPh_2)_4]$ (**9**) was synthesized by heating an acetonitrile solution of $[Ph_4P]_2[NpCl_6]$ with two equivalents of $[K(Se_2PPh_2)]_2$ (Scheme 4) in MeCN with heating, and isolated in 29% crystalline yield. The ^{31}P NMR spectrum of **9** dissolved in CD_2Cl_2 revealed a single broad resonance at −902 ppm. We did not attempt to prepare a Pu^{IV} complex with the $[Se_2PPh_2]^-$ ligand because preliminary Pu^{IV} reactions of $[Ph_4P]_2[PuCl_6]$ with the $[S_2PPh_2]^-$ ligand, in a separate project, have indicated at least partial reduction of Pu^{IV} to Pu^{III} suspected to arise from ligand dimerization through the formation of a disulfide bond, and the products were intractable.[40] Given that a diselenide bond would likely also form under similar conditions, attempting the analogous $[Se_2PPh_2]^-$ reaction with Pu^{IV} was not deemed to be a judicious use of our limited Pu isotope supplies.

Very dark green, X-ray diffraction quality crystals of **9** were grown by layering MeCN onto a THF solution of the complex. Structural characterization of both **8** and **9** reveals isostructural complexes in the monoclinic $P2_1$ space group (Table 6). Both complexes feature an eight-coordinate metal center with four $[Se_2PPh_2]^-$ ligands, each bound to the metal through both Se atoms (Fig. 5). The geometry about the An^{IV} ions is probably best described as distorted bicapped trigonal prismatic, with gaps between the 17th and 18th lowest ligand–metal–ligand angles of 18.35° in **8** and 16.64° in **9**. A list of An–Se bond distances for **8** and **9** are presented in Table 5 (listed from longest to shortest), together with metal–ligand bond lengths obtained from DFT calculations on model compounds **8a** and **9a**, and also on analogous Th (**10a**), Pa (**11a**) and Pu (**12a**) species. Although no symmetry constraints were imposed on the calculations, the An–Se bonds clearly separate into two groups, within which the metal–ligand distances are essentially identical in all cases bar the Np model **9a**, which shows a slight variation within the groups. The experimental data for **8** and **9** also indicate that there are four longer An–Se bonds and four shorter bonds, though the variation within the groups is more pronounced than found computationally. The computed data reveal a shortening of An–Se from Th to Pa, beyond which there

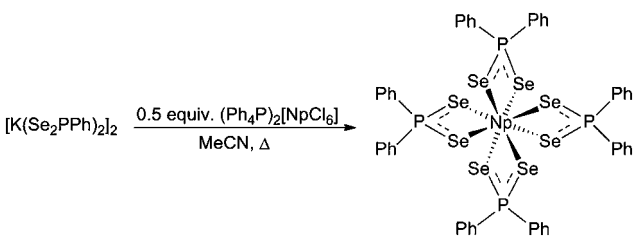

Scheme 4 Synthesis of the 1 : 4 metal–ligand complex $[Np(Se_2PPh_2)_4]$ (**9**).

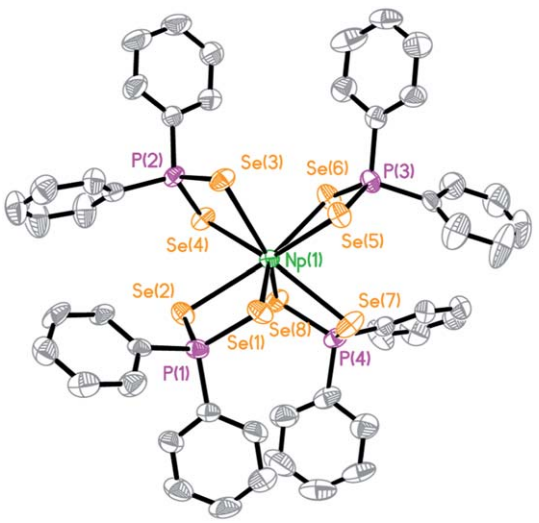

Fig. 5 Solid-state structure of $[Np(Se_2PPh_2)_4]$ (**9**). Hydrogen atoms are omitted for clarity. Thermal ellipsoids are shown at the 50% probability level. The U^{IV} analog, **8**, is isostructural.

Table 5 Selected experimental bond distances (Å), for $[U(Se_2PPh_2)_4]$ (**8**) and $[Np(Se_2PPh_2)_4]$ (**9**), and calculated data for model compounds **8a**, **9a**, **10a** (Th), **11a** (Pa) and **12a** (Pu) in italics[a]

Bond	10a	11a	8/8a	9/9a	12a	Δ(8–9)
M–Se_1	*3.084*	*3.056*	3.0503(4) *3.044*	3.0320(8) *3.053*	*3.050*	0.0183
M–Se_2	*3.083*	*3.056*	3.0296(4) *3.043*	3.0200(8) *3.042*	*3.050*	0.0096
M–Se_3	*3.083*	*3.056*	3.0275(4) *3.043*	3.0190(8) *3.022*	*3.050*	0.0085
M–Se_4	*3.083*	*3.056*	3.0266(4) *3.043*	3.0107(9) *3.021*	*3.049*	0.0159
M–Se_5	*3.022*	*2.976*	2.9401(4) *2.945*	2.9205(9) *2.955*	*2.936*	0.0196
M–Se_6	*3.022*	*2.976*	2.9066(4) *2.945*	2.9040(8) *2.949*	*2.936*	0.0026
M–Se_7	*3.022*	*2.976*	2.8989(4) *2.945*	2.8848(8) *2.932*	*2.936*	0.0141
M–Se_8	*3.022*	*2.976*	2.8817(4) *2.945*	2.8766(8) *2.931*	*2.936*	0.0051

[a] Avg Δ, (U–Se)–(Np–Se): 0.0120, *0.005*.

is rather less variation in metal–ligand distance as a function of metal, in agreement with the data for **8** and **9**. The experimental U–Se bonds range from 3.0503(4) to 2.8817(4) Å and the Np–Se bonds lie between 3.0320(8) and 2.8766(8) Å. The average difference in bond lengths between **8** and **9** is just 0.012 Å, close to the computed average difference of 0.005 Å. These differences are less than the difference in reported ionic radii for eight-coordinate U^{IV} (1.00 Å) and Np^{IV} (0.98 Å), suggesting that there is little difference in the nature of the metal–ligand bonding between U and Np, *i.e.* that the An–Se bond length changes from **8** to **9** are adequately rationalised by the actinide contraction.

Vis-NIR spectroscopy

The radioactivity of ^{237}Np and ^{239}Pu places some limitations on the range of characterization techniques that are approved for use with these isotopes. In particular, elemental analysis is usually conducted by an external user facility that is not equipped or approved to handle high specific-activity α-particle emitters. One technique that we have found to be useful in providing additional fingerprint characterization on solid transuranic complexes is diffuse reflectance electronic absorption spectroscopy.[29,41–45] Comparison of the solid-state vis-NIR spectra of **5**, **7**, and **9** show good correlation of the 5f-6d and 5f-5f electronic transitions to those observed in solution (Fig. 6 and ESI†), providing support for identical speciation between the two phases. There are some relatively small differences between solid and solution phases which are attributed to either the different resolutions of the solid *versus* solution data acquisition parameters/instrumentation and/or differences in the local solid *versus* solution metal coordination geometry/symmetry. Particular differences worthy of mention in this study are that for complex **7** there is an apparent slight red-shift of the bands upon moving from the solution to the solid phase.

Electronic structure

We have recently devoted considerable effort to probing changes in the metal–ligand bonding as a function of actinide from Th through to the so-called minor actinides Am and Cm.[23,27,30,31] As noted in the Introduction, these studies have called into question the exclusive use of the more traditional measures of assessing covalency (*e.g.* MO compositions and spin densities) as the energetic proximity of metal valence 5f and ligand orbitals can result in MOs with significant contributions from both atoms, yet little spatial overlap, yielding highly mixed orbitals but no significant internuclear build-up of electron density. Fig. 7 presents valence MO energy level diagrams for **8a–12a**, and nicely illustrates a typical feature of the electronic structure of molecules containing the early actinide elements; while the energies of the largely ligand-based orbitals do not alter appreciably from Th to Pu, there is a very pronounced stabilization (and radial contraction) of the metal 5f-based orbitals (shown in blue) from **11a** (Pa) to **12a** (Pu). The significant number of green lines in the U, Np and Pu systems, indicating MOs with >10% but <50% metal f character, arises (certainly for the latter two cases) primarily from the degeneracy of the metal and ligand valence functions, and does not imply large overlaps, as discussed previously.[23,27,30,31] This has consequences for the metals' atomic spin densities, where the largest deviations from formal values are found in those compounds with the largest orbital mixing. The formal spin density deviations for **11a**, **8a**, **9a** and **12a** are shown in Fig. 8; clearly the Pu has a very significant deviation from the formal value, but this should not be taken to indicate that **12a** features the most covalent metal–ligand bond (other than in a strict orbital mixing sense).

The 5f orbitals are not, of course, the only valence functions of the early actinide elements, and several authors have suggested the participation of the 6d orbitals in covalent bonding (see ref. 38 for a recent example). In **10a** the lowest energy 6d-based MO is barely bound, lying at −0.38 eV (5.33 eV above the HOMO) a situation largely unaltered across the target systems (in **12a**, the gap between the HOMO and the lowest 6d-based orbital is 5.62 eV, and that between the (occupied) 5f- and (unoccupied) 6d-based orbitals is 7.90 eV). These rather large 6d/ligand energy gaps are not conducive to significant covalency, notwithstanding that Fig. 7 indicates that **8a–12a** each have several occupied MOs with c. 10% metal d contribution.

An alternative approach to assessing covalency, which we have recently begun to apply to computationally derived f element charge densities, is the quantum theory of atoms in molecules (QTAIM).[46] We have discussed elsewhere some of the key features of this approach,[30] which is also beginning to be employed experimentally in actinide chemistry,[47] and will not repeat them here, except to note that chemical bonding interactions may be characterized and classified according to the properties of the bond critical points (BCPs); for example the electron and energy densities ρ and H. A representative molecular graph (for **10a**), showing the location of the bond paths and BCPs, is provided in Fig. 9.

ρ and H for the An–Se BCPs are presented in Fig. 10. As we have seen previously for the actinides, the data indicate that all

Table 6 Selected crystallographic data collection and refinement details for complexes **1–9**

	$[La(Se_2PPh_2)_3(THF)_2]\cdot 0.5$hexane (**1**)	$[Ce(Se_2PPh_2)_3(THF)_2]$ (**2**)	$[Nd(Se_2PPh_2)_3(THF)_2]\cdot 0.5$hexane (**3**)	$[La(Se_2PPh_2)_3(MeCN)_2]$ (**4**)	$[Pu(Se_2PPh_2)_3(THF)_2]$ (**5**)	$[Et_4N][Ce(Se_2PPh_2)_4]\cdot$THF (**6**)	$[Et_4N][Pu(Se_2PPh_2)_4]\cdot$THF (**7**)	$[U(Se_2PPh_2)_4]$ (**8**)	$[Np(Se_2PPh_2)_4]$ (**9**)
Empirical formula	$C_{47}H_{53}LaO_2P_3Se_6$	$C_{44}H_{46}CeO_2P_3Se_6$	$C_{47}H_{53}NdO_2P_3Se_6$	$C_{40}H_{36}LaN_2P_3Se_6$	$C_{44}H_{46}PuO_2P_3Se_6$	$C_{60}H_{68}CeNOP_4Se_8$	$C_{60}H_{68}PuNOP_4Se_8$	$C_{48}H_{40}UP_4Se_8$	$C_{48}H_{40}NpP_4Se_8$
Crystal habit, color	Colorless blocks	Colorless blocks	Pale blue blocks	Colorless plates	Blue blocks	Yellow blocks	Dark green plates	Green blocks	Black plates
Crystal size (mm)	0.16 × 0.10 × 0.10	0.18 × 0.12 × 0.10	0.14 × 0.14 × 0.12	0.12 × 0.10 × 0.05	0.16 × 0.16 × 0.14	0.28 × 0.14 × 0.08	0.42 × 0.30 × 0.08	0.34 × 0.16 × 0.08	0.16 × 0.08 × 0.06
Crystal system	Tetragonal	Triclinic	Tetragonal	Monoclinic	Triclinic	Orthorhombic	Orthorhombic	Monoclinic	Monoclinic
Space group	$P4_2/nmc$	$P\bar{1}$	$P4_2/nmc$	$P2_1/c$	$P\bar{1}$	$P2_12_12_1$	$P2_12_12_1$	$P2_1$	$P2_1$
V(Å^3)	10 657(3)	2301(5)	10 541(15)	4346(6)	4747(2)	6393(5)	6400(11)	2550(2)	2611(6)
a (Å)	31.601(4)	9.8457(13)	31.4695(18)	13.5653(10)	13.344(4)	12.6878(5)	12.7053(12)	13.8131(6)	13.8899(19)
b (Å)	31.601(4)	13.0684(17)	31.4695(18)	9.0111(7)	18.862(5)	21.9927(9)	21.997(2)	9.7933(5)	9.9688(14)
c (Å)	10.671(3)	19.024(2)	10.6442(12)	35.576(3)	20.428(5)	22.9089(10)	22.902(2)	18.8547(9)	18.862(3)
α (°)	90.00	88.600(1)	90.00	90.00	79.465(4)	90.00	90.00	90.00	90.00
β (°)	90.00	85.615(1)	90.00	91.945(1)	89.356(4)	90.00	90.00	91.597(1)	91.609(2)
γ (°)	90.00	70.493(1)	90.00	90.00	70.120(3)	90.00	90.00	90.00	90.00
Z	8	2	8	4	4	4	4	2	2
Formula weight (g mol^{-1})	1355.47	1313.63	1360.80	1250.31	1412.53	1714.88	1813.76	1610.41	1609.41
Final R indices [$I > 2\sigma(I)$]	$R_1 = 0.0831$ w$R_2 = 0.1840$	$R_1 = 0.0323$ w$R_2 = 0.0685$	$R_1 = 0.0381$ w$R_2 = 0.0732$	$R_1 = 0.0390$ w$R_2 = 0.0817$	$R_1 = 0.0703$ w$R_2 = 0.1556$	$R_1 = 0.0269$ w$R_2 = 0.0461$	$R_1 = 0.0261$ w$R_2 = 0.0448$	$R_1 = 0.0226$ w$R_2 = 0.0463$	$R_1 = 0.0414$ w$R_2 = 0.0622$

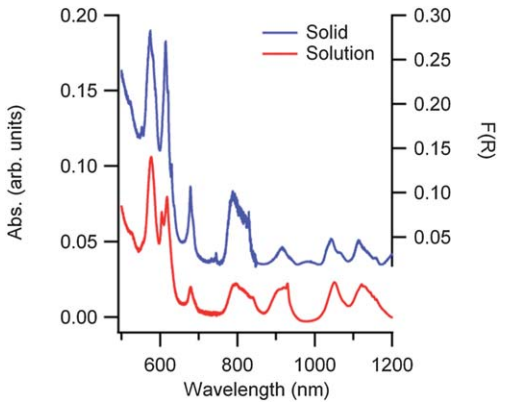

Fig. 6 Visible/near-IR spectra of solid-state **5** (blue, top) and **5** dissolved in CH_2Cl_2 solution (bottom, red). See the ESI† for the corresponding spectra of **7** and **9**.

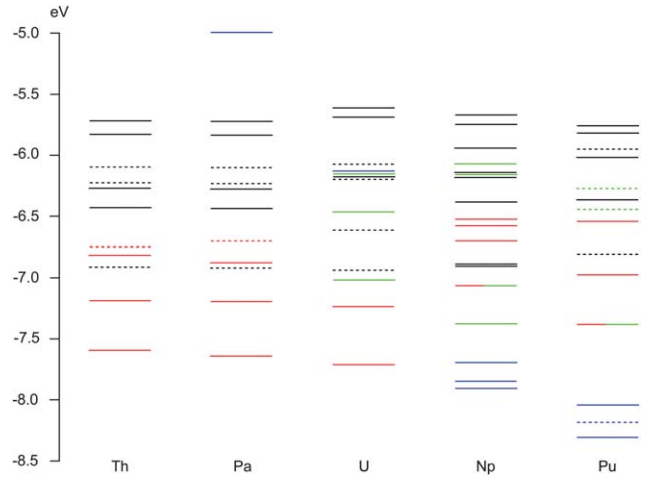

Fig. 7 Energy level diagrams for the highest occupied valence molecular orbitals of $[An(Se_2PMe_2)_4]$ (An = Th (**10a**), Pa (**11a**), U (**8a**), Np (**9a**) and Pu (**12a**)). Dashed lines indicate two almost degenerate orbitals. Red lines indicate MOs with 10–15% metal d character, green = MOs with >10% metal f character, blue = MOs with >50% metal f character.

of the bonds are predominantly ionic, and the trend as function of metal is also similar to what we have seen before.[27,29,30,48,49] The electron density at the BCP increases from Th to U, and

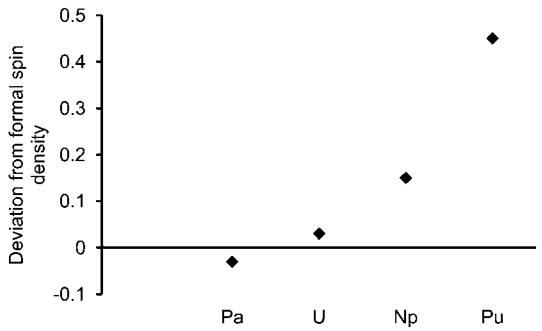

Fig. 8 Hirshfeld metal spin densities for $[An(Se_2PMe_2)_4]$ (An = Pa (**11a**), U (**8a**), Np (**9a**) and Pu (**12a**)). Values quoted are the differences from the formal value for An(IV).

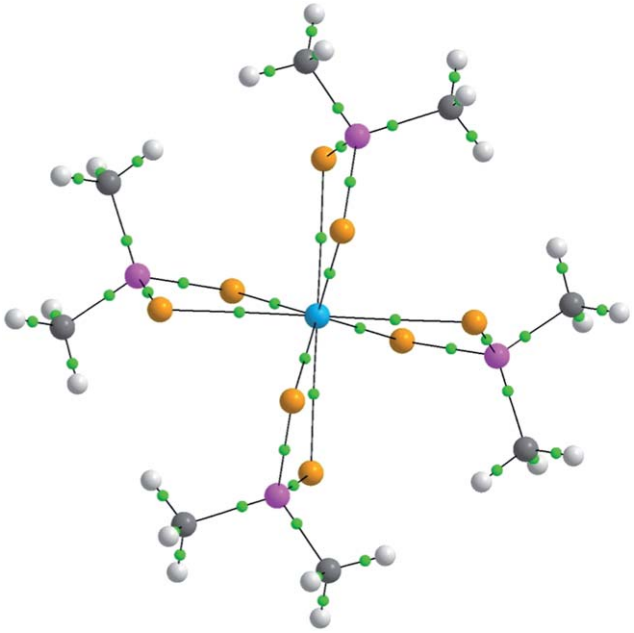

Fig. 9 Molecular graph of $[Th(Se_2PMe_2)_4]$ (**10a**). Th: blue, Se: orange, P: magenta, C: grey, H: white, bond critical points: green, bond paths: grey.

then decreases slightly to Np and Pu, suggesting that the U–Se bond is the most covalent. A similar conclusion can be drawn from the energy density data; H at the BCP is negative for interactions with significant sharing of electrons, its magnitude

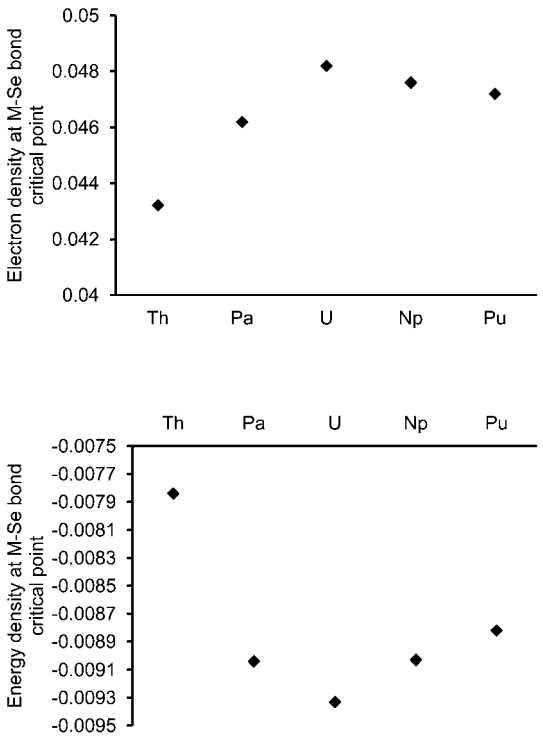

Fig. 10 Electron (upper, e $bohr^{-3}$) and energy (lower, H $bohr^{-3}$) densities for $[An(Se_2PMe_2)_4]$ (An = Pa (**11a**), U (**8a**), Np (**9a**) and Pu (**12a**)) at the An–Se bond critical points. The data are the average of the values at the four shorter An–Se bonds.

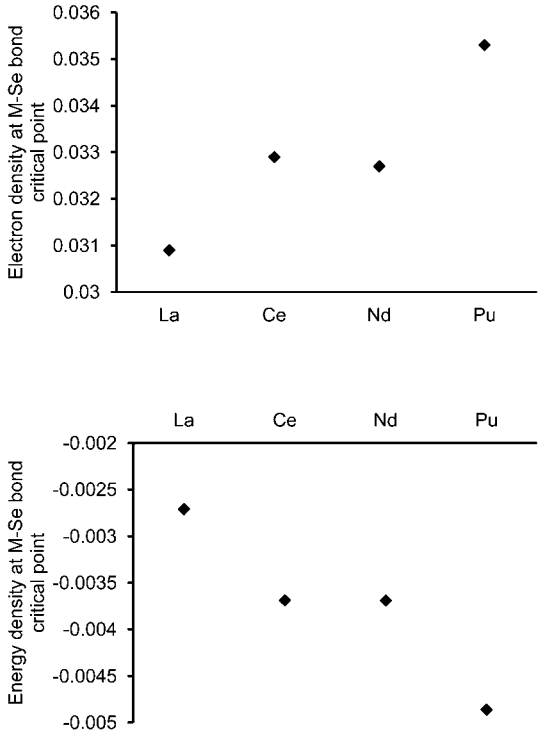

Fig. 11 Electron (upper, e bohr^{-3}) and energy (lower, H bohr^{-3}) densities for $[M(Se_2PMe_2)_3(THF)_2]$ (M = La (**1a**), Ce (**2a**), Nd (**3a**) and Pu (**5a**)) at the M–Se bond critical points. The data are the average of the values at the three shorter An–Se bonds.

reflecting the "covalence" of the interaction.[50] The small differences between the U and Np data are entirely in keeping with the very small bond length differences observed experimentally and computationally.

We have also performed QTAIM analysis of the trivalent model compounds **1a**, **2a**, **3a** and **5a**, particularly to assess if the structural data presented earlier do indeed indicate a slightly larger covalent contribution to the Pu–Se bond *versus* the Ce analogue. Fig. 11 suggests that this is indeed the case, with slightly larger electron and energy densities at the Pu–Se BCP. This conclusion is reinforced by the QTAIM-derived atomic charges. The difference between the metal and average Se value is 2.64, 2.60 and 2.59 for the La, Ce and Nd compounds respectively, a little larger than the 2.48 calculated for $[Pu(Se_2PMe_2)_3(THF)_2]$.

Conclusion

A series of 4f and 5f metal complexes with the bidentate diselenophosphinate ligand $[Se_2PPh_2]^-$ have been synthesized and characterized both structurally and spectroscopically. Both 1 : 3 solvento adducts $[M(Se_2PPh_2)_3(THF)_2]$ (M = Ce, Pu) and 1 : 4 homoleptic complexes $[Et_4N][M(Se_2PPh_2)_4]$ (M = Ce, Pu) were compared. Overall the Pu–Se bonds are consistently shorter than corresponding Ce–Se bonds, with the isostructural 1 : 4 complexes providing the most meaningful data that are consistent with the postulation of a modest enhancement of covalency in Pu–Se *versus* Ce–Se bonding. These findings are of relevance to structurally related S donor dithiophosphinate extractant ligands, for which the chemical basis of their actinide selectivity is still under debate but suspected to originate from differential covalent bonding contributions. Two isostructural An^{IV} complexes, $[An(Se_2PPh_2)_4]$ (An = U, Np), were also characterized and appear to follow bonding trends that would be expected as a result of the actinide contraction, consistent with ionic bonding models.

Computationally derived geometries of model compounds, in which the Ph groups were replaced by Me groups, support experimental data in finding consistently shorter Pu–Se than Ce–Se bonds. Analysis of the electronic structure has focused on the use of the quantum theory of atoms-in-molecules, initially on the model series of An(IV) systems $[An(Se_2PMe_2)_4]$ (An = Th–Pu) and then on trivalent $[M(Se_2PMe_2)_3(THF)_2]$ (M = La, Ce, Nd, Pu). The electron and energy densities at the M–Se bond critical points indicate that, while the An(IV)–Se bonds are all rather ionic, the U–Se bond is the least so. The QTAIM data for $[U(Se_2PMe_2)_4]$ and $[Np(Se_2PMe_2)_4]$ are rather similar to one another, supporting the conclusion based on computational and experimental structural data of there being little difference in the An–Se bonding in this part of the 5f series. Comparison of the metrics of the Pu–Se and Ce–Se BCPs in $[M(Se_2PMe_2)_3(THF)_2]$ supports the suggestion that the former is slightly the more covalent.

Overall, we have provided new insight into the coordination chemistry and bonding of dichalcogenophosphinates with the f-elements by employing a 'softer' selenium donor relation of sulphur donor actinide extractant molecules. The knowledge gained in this study has potential for future exploitation in the design, optimization, and understanding of actinide separation schemes. Finally, the syntheses, spectroscopic, and structural elucidation of three new non-aqueous transuranic molecules is a rare addition of significant impact to the field in helping to bridge the chasm between the large body of non-aqueous complexes reported for the 4f elements and U/Th compared to the dearth of non-aqueous transuranic molecules. In fact, the lack of well characterized transuranic complexes (structural determinations along with other spectroscopic probes will be required for an in-depth understanding) is one contributing factor as to why conclusive interpretation of existing metrical data is very difficult and complicated.

Experimental

General information

All manipulations of lanthanide compounds were carried out using standard Schlenk techniques or conducted in a MBraun UniLab glovebox under an argon atmosphere. The manipulation of transuranic elements was performed in a negative pressure MBraun Labmaster 130 glovebox under a helium atmosphere. All reagents were purchased from commercial vendors and used as received, unless otherwise noted. α-phase plutonium metal pieces of weapons-grade isotopic composition, uranium turnings (depleted in ^{235}U), and acidic stock solutions of neptunium (purified by anion exchange chromatography) were obtained internally from Los Alamos National Laboratory. $[K(Se_2PPh_2)]_2$,[32]

$[PuI_3(py)_4]$,[51] and $[Ph_4P]_2[NpCl_6]$,[52] were all prepared according to the literature. Anhydrous solvents were purchased from Sigma-Aldrich and further purified by sparging with argon gas, followed by storage over 3 Å molecular sieves. Deuterated NMR solvents were purchased from Cambridge Isotope Laboratories and degassed and dried over 3 Å molecular sieves. Elemental analyses were performed by Midwest Microlabs, Indianapolis, IN. ^{1}H and ^{31}P NMR spectra were recorded on Bruker Avance 300 MHz or Bruker Avance 400 MHz spectrometers at ambient temperature. Chemical shifts were referenced to residual solvent peaks for ^{1}H NMR spectra and externally referenced to 85% H_3PO_4 for ^{31}P NMR spectra. All NMR spectra of actinide-containing compounds were obtained in 4 mm PTFE NMR tube liners inserted into 5 mm NMR tubes in order to multiply contain the radioactive samples. Infrared spectra were recorded as Nujol mulls on NaCl plates on a Nicolet Magna-IR 560 spectrometer. Electronic absorption spectra were recorded on either a Varian 6000i UV/vis/NIR spectrophotometer (solution) using 1 cm path length quartz cuvettes or a Cary 500 UV/vis/NIR spectrophotometer (solid).

Syntheses

Caution! ^{239}Pu and ^{237}Np are high specific-activity α-particle-emitting radionuclides. This research was conducted in a radiological facility with appropriate analyses of hazards and implementation of controls for the safe handling and manipulation of radioactive materials.

$[La(Se_2PPh_2)_3(THF)_2]$ (1). $[K(Se_2PPh_2)]_2$ (0.080 g, 0.105 mmol) was dissolved in THF (5 mL). $La(OTf)_3$ (0.041 g, 0.070 mmol) was added as a solid, and the suspension was heated to 60 °C with stirring for one hour. The resultant homogenous mixture was cooled and concentrated to dryness. The colorless residue was taken up in toluene (2 mL) and filtered to remove KOTf. Hexanes was diffused into the toluene filtrate to give colorless X-ray quality crystals of $[La(Se_2PPh_2)_3(THF)_2]$ that were collected and dried *in vacuo* (0.055 g, 59% yield). ^{1}H (δ, $CDCl_3$, 400 MHz): 7.94–7.89 (m, 12H, ArH), 7.36 (bs, 18H, ArH), 3.92 (m, 8H, THF), 1.70 (m, 8H, THF). $^{31}P\{^1H\}$ (δ, $CDCl_3$, 400 MHz): 16.50. FT-IR (thin film, cm^{-1}): 3068, 3051, 2974, 2875, 1963, 1893, 1813, 1774, 1722, 1646, 1584, 1572, 1479, 1435, 1306, 1182, 1092, 1067, 1053, 1026, 999, 913, 867, 744, 691. Anal. calcd for $[La(Se_2PPh_2)_3(THF)_2]$: C, 40.27; H, 3.53. Found: C, 40.43; H, 3.51%.

$[Ce(Se_2PPh_2)_3(THF)_2]$ (2). This compound was prepared in a similar fashion to $[La(Se_2PPh_2)_3(THF)_2]$ using $[K(Se_2PPh_2)]_2$ (0.075 g, 0.098 mmol) and $CeBr_3$ (0.025 g, 0.065 mmol) to give $[Ce(Se_2PPh_2)_3(THF)_2]$ as a yellow, crystalline solid (0.034 g, 40% yield). X-ray quality crystals were obtained by vapor diffusion of hexanes into a toluene solution of $[Ce(Se_2PPh_2)_3(THF)_2]$. ^{1}H (δ, $CDCl_3$, 400 MHz): 8.88, 7.71, 7.68, 3.18, 2.24. $^{31}P\{^1H\}$ (δ, $CDCl_3$, 400 MHz): −58.27. FT-IR (thin film, cm^{-1}): 3068, 3051, 2974, 2874, 1963, 1892, 1812, 1773, 1647, 1584, 1572, 1479, 1435, 1306, 1182, 1092, 1067, 1052, 1026, 998, 913, 866, 744, 691. Anal. calcd for $[Ce(Se_2PPh_2)_3(THF)_{0.5}]$: C, 37.86; H, 2.84. Found: C, 37.84; H, 3.04%.

$[Nd(Se_2PPh_2)_3(THF)_2]$ (3). This compound was prepared in a similar fashion to $[La(Se_2PPh_2)_3(THF)_2]$ using $[K(Se_2PPh_2)]_2$ (0.075 g, 0.098 mmol) and $NdCl_3$ (0.016 g, 0.065 mmol) to give $[Nd(Se_2PPh_2)_3(THF)_2]$ as a pale blue, crystalline solid (0.065 g, 75% yield). X-ray quality crystals were obtained by vapor diffusion of hexanes into a toluene solution of $[Nd(Se_2PPh_2)_3(THF)_2]$. ^{1}H (δ, $CDCl_3$, 400 MHz): 9.34, 7.82, 7.74, 0.37, −2.35. $^{31}P\{^1H\}$ (δ, $CDCl_3$, 400 MHz): −279.46. FT-IR (thin film, cm^{-1}): 3069, 3051, 2974, 2874, 1963, 1893, 1814, 1775, 1723, 1647, 1584, 1573, 1479, 1435, 1306, 1182, 1092, 1067, 1026, 999, 912, 866, 745, 691. Anal. calcd for $[Nd(Se_2PPh_2)_3(THF)_{0.5}]$: C, 37.73; H, 2.83. Found: C, 37.69; H, 2.95%.

$[La(Se_2PPh_2)_3(MeCN)_2]$ (4). This compound was prepared in a similar fashion to $[La(Se_2PPh_2)_3(THF)_2]$ using $[K(Se_2PPh_2)]_2$ (0.050 g, 0.065 mmol) and $La(OTf)_3$ (0.026 g, 0.044 mmol) in acetonitrile (5 mL) to give $[La(Se_2PPh_2)_3(MeCN)_2]$ as a colorless, crystalline solid (0.038 g, 70% yield). X-ray quality crystals were obtained by vapor diffusion of diethyl ether into an acetonitrile (with a few drops of THF) solution of $[La(Se_2PPh_2)_3(MeCN)_2]$. ^{1}H (δ, $CDCl_3$, 400 MHz): 7.96–7.85 (m, 12H, ArH), 7.35 (bs, 18H, ArH), 1.82 (s, 6H, MeCN). $^{31}P\{^1H\}$ (δ, $CDCl_3$, 400 MHz): 17.38. FT-IR (thin film, cm^{-1}): 3070, 3052, 2982, 2877, 2266, 1964, 1900, 1815, 1647, 1615, 1478, 1434, 1306, 1181, 1091, 1067, 1027, 998, 869, 745, 691. Anal. calcd for $[La(Se_2PPh_2)_3(MeCN)_2]$: C, 38.42; H, 2.90; N, 2.24. Found: C, 38.68; H, 2.98; N, 2.22%.

$[Pu(Se_2PPh_2)_3(py)_2]$. $PuI_3(py)_4$ (0.018 g, 0.019 mmol) was dissolved in pyridine (3 mL). $[K(Se_2PPh_2)]_2$ (0.022 g, 0.029 mmol) was added as a solid, and the suspension was heated to 60 °C with stirring for one hour. The resultant heterogeneous mixture was cooled and concentrated to dryness. The brown-green residue was taken up in toluene (1 mL) and filtered. Hexanes (5 mL) were added to the filtrate with stirring causing precipitation of the product as a pale green solid. The solvent was decanted from the solid, which was washed with an additional portion of hexanes (5 mL). The hexanes were decanted and the remaining pale green solid was dried *in vacuo* (0.011 g, 41% yield). ^{1}H (δ, CD_2Cl_2, 300 MHz): 8.57, 7.78, 7.69, 7.37, 7.25, 7.06. $^{31}P\{^1H\}$ (δ, CD_2Cl_2, 300 MHz): −179. Visible/near-IR (CH_2Cl_2 solution, nm): 576, 604, 618, 679, 795 (br), 916 (br), 930, 1051 (br), 1121 (br); visible/near-IR (solid-state diffuse reflectance, nm): 575, 614, 630, 678, 788 (br), 915 (br), 1041 (br), 1113 (br).

$[Pu(Se_2PPh_2)_3(THF)_2]$ (5). This compound was prepared in a similar fashion to $[Pu(Se_2PPh_2)_3(py)_2]$ using $[K(Se_2PPh_2)]_2$ (0.021 g, 0.027 mmol) and $PuI_3(py)_4$ (0.017 g, 0.018 mmol) in THF (3 mL). X-ray quality crystals were obtained through fractional crystallization of $[Pu(Se_2PPh_2)_3(THF)_2]$ from $[Pu(Se_2PPh_2)_3(py)_2]$ by vapor diffusion of hexanes into a 1 : 1 toluene–THF mixture to give blue crystals of $[Pu(Se_2PPh_2)_3(THF)_2]$. ^{1}H (δ, CD_2Cl_2, 300 MHz): 8.57, 7.87, 7.65, 7.35, 7.23, 6.98, 3.48, 1.65. $^{31}P\{^1H\}$ (δ, CD_2Cl_2, 300 MHz): −184.

$[Et_4N][Ce(Se_2PPh_2)_4]$ (6). $CeBr_3$ (0.012 g, 0.033 mmol) was dissolved in hot THF (5 mL) with stirring. Solvent was removed *in vacuo* and the colorless residue was dissolved in MeCN (5 mL). $[K(Se_2PPh_2)]_2$ (0.050 g, 0.065 mmol) was added as a solid. When all solid had dissolved, Et_4NBr (0.007 g, 0.033 mmol) was added as a solid, and the mixture was heated to 60 °C with stirring for one hour. The resultant mixture was cooled and concentrated to dryness. The yellow residue was taken up in THF (2 mL) and filtered to remove KBr. Et_2O was diffused into the THF filtrate to

give pale yellow, X-ray quality crystals of $[Et_4N][Ce(Se_2PPh_2)_4]$, that were collected and dried *in vacuo* (0.029 g, 54% yield). ^1H (δ, THF-d_8, 400 MHz): 7.46, 7.08, 3.28 (q, 8H, Et_4N^+), 1.17 (t, 12H, Et_4N^+). $^{31}P\{^1H\}$ (δ, THF-d_8, 400 MHz): −68.12. FT-IR (thin film, cm^{-1}): 3067, 3049, 2975, 2866, 1964, 1894, 1813, 1771, 1645, 1584, 1572, 1479, 1435, 1392, 1305, 1181, 1093, 1066, 1027, 999, 906, 746, 691. Anal. calcd for $[Et_4N][Ce(Se_2PPh_2)_4]\cdot THF$: C, 42.02; H, 4.00; N, 0.82. Found: C, 42.09; H, 3.95; N, 0.90%.

$[Et_4N][Pu(Se_2PPh_2)_4]$ (7). $PuI_3(py)_4$ (0.013 g, 0.014 mmol) was dissolved in MeCN (3 mL) with stirring. $[K(Se_2PPh_2)]_2$ (0.022 g, 0.029 mmol) was added as a solid. When all solid had dissolved, Et_4NBr (0.003 g, 0.014 mmol) was added as a solid, and the mixture was heated to 60 °C with stirring for 1 hour. The resultant mixture was cooled and concentrated to dryness. The green-brown residue was taken up in dichloromethane (2 mL), filtered to remove K^+ salts, and the filtrate was concentrated to dryness. The residue was recrystallized by vapor diffusion of diethyl ether into a 1 : 1 THF–MeCN solution of the product to give green, X-ray quality crystals of $[Et_4N][Pu(Se_2PPh_2)_4]$ (0.013 g, 52% yield). ^1H (δ, THF-d_8, 300 MHz): 8.14, 7.29, 3.29 (q, 8H, Et_4N^+), 1.16 (t, 12H, Et_4N^+). $^{31}P\{^1H\}$ (δ, THF-d_8, 300 MHz): −170 ppm. Visible/near-IR (THF solution, nm): 571, 611, 675, 785 (br), 821 (br), 907 (br), 1037 (br), 1063 (br), 1112 (br); visible/near-IR (solid-state diffuse reflectance, nm): 575, 618, 683, 802 (br), 917 (br), 1058 (br), 1133 (br).

$[U(Se_2PPh_2)_4]$ (8). $UI_3(THF)_4$ (0.0500 g, 0.055 mmol) was dissolved in THF (5 mL) with stirring. $[K(Se_2PPh_2)]_2$ (0.0692 g, 0.083 mmol) was dissolved in THF (2 mL) and added to the uranium-containing solution causing a color change to brown-green. The reaction mixture was stirred at ambient temperature for 2.5 hours and then filtered to remove precipitates. Volatiles were removed *in vacuo* from the filtrate and the residue dissolved in benzene (2 mL). Vapor diffusion of Et_2O into the benzene solution resulted in deposition of a few green crystals of X-ray diffraction quality. A pure bulk sample for elemental analysis could not be obtained. The NMR data was collected on a sample *in situ* and not from the dissolution of a pure, isolated, solid sample. ^1H (δ, C_6D_6, 300 MHz): 12.22, 8.90, 8.59. $^{31}P\{^1H\}$ (δ, C_6D_6, 300 MHz): −810.

$[Np(Se_2PPh_2)_4]$ (9). $[K(Se_2PPh_2)]_2$ (0.023 g, 0.030 mmol) was dissolved in THF (3 mL) with stirring, and $[Ph_4P]_2[NpCl_6]$ (0.017 g, 0.015 mmol) was added as a solid. The mixture was heated to 60 °C with stirring for one hour. The resultant dark green-brown mixture was cooled, filtered over a pad of Celite, and the filtrate was concentrated to dryness. The residue was washed with 2 × 2 mL portions of acetonitrile, and the solid $[Np(Se_2PPh_2)_4]$ was dried *in vacuo*. X-ray quality crystals of $[Np(Se_2PPh_2)_4]$ were obtained by layering acetonitrile on top of a THF solution of the product (0.007 g, 29% yield). ^1H (δ, CD_2Cl_2, 300 MHz): 9.51, 8.11. $^{31}P\{^1H\}$ (δ, CD_2Cl_2, 300 MHz): −902. Visible/near-IR (THF solution, nm): 555 (br), 595 (br), 902 (br), 975 (sh, br), 1008 (br), 1054 (br); visible/near-IR (solid-state diffuse reflectance, nm): 591 (br), 623 (br), 910 (br), 976 (sh), 1012 (br), 1054 (br).

X-ray crystallographic data collection and refinement details

Lanthanide and uranium crystals. The crystals were mounted in a nylon cryoloop using Paratone-N oil under argon gas flow. The data were collected on a Bruker SMART APEX II charge-coupled-device (CCD) diffractometer, at a temperature of 120(1) K with a Cryo Industries of America Cryocool G2 cooling device. The instrument was equipped with graphite monochromatized MoKα X-ray source (λ = 0.71073 Å), with MonoCap X-ray source optics. A hemisphere of data was collected using ω scans, with 10 second frame exposures and 0.3° frame widths. Data collection and initial indexing and cell refinement were handled using APEX II software.[53] Frame integration, including Lorentz-polarization corrections, and final cell parameter calculations were carried out using SAINT+ software.[54] The data were corrected for absorption using the SADABS program.[55] Decay of reflection intensity was monitored *via* analysis of redundant frames. The structure was solved using direct methods and difference Fourier techniques. All hydrogen atom positions were idealized, and rode on the atom they were attached to. Structure solution, refinement, graphics, and creation of publication materials were performed using SHELXTL.[56] The program PLATON-SQUEEZE was used to remove disordered solvent molecules from the unit cell where appropriate and details are in the crystallographic files.[57] Compound **6** is a chiral propeller-like molecule and the crystal was racemically pure with the Flack parameter refining to a value of zero (within a few esd's).

Plutonium and neptunium crystals. The crystals were placed in Paratone-N oil and mounted in a 0.5 mm X-ray capillary tube, sealed with hot wax, and an acrylic coat applied to provide additional containment of the crystal. The reflection data were collected on a Bruker Platform diffractometer with 1k CCD, at a temperature of 140(1) K with Bruker Kryoflex cryostat. The instrument was equipped with a sealed, graphite monochromatized MoKα X-ray source (λ = 0.71073 Å). A hemisphere of data was collected using φ scans, with 30 second frame exposures and 0.3° frame widths. Data collection and initial indexing and cell refinement were handled using SMART software.[58] Frame integration, including Lorentz-polarization corrections, and final cell parameter calculations were carried out using SAINT software.[59] The data were corrected for absorption using the SADABS program.[55] Decay of reflection intensity was monitored *via* analysis of redundant frames. The structure was solved using direct methods and difference Fourier techniques. Structure solution, refinement, graphics, and creation of publication materials were performed using SHELXTL.[60] For compound **5**, temperature factor restraints were used on 6 carbon atoms to force convergence. Compound **7** is a chiral propeller-like molecule and the crystal was racemically pure with the Flack parameter refining to a value of zero (within a few esd's).

Computational details. Hybrid density functional theory calculations were carried out using the PBE0 functional,[61] as implemented in the Gaussian 09 Rev. A.02 (G09) quantum chemistry code.[62] Spin-unrestricted calculations were performed on all open shell molecules; the formal f^n configurations of M(III) are n = 1 (Ce), 3 (Nd) and 5 (Pu) and, for An(IV), n = 1 (Pa), 2 (U), 3 (Np) and 4 (Pu). The "ultrafine" integration grid was employed for all calculations, together with the default geometry convergence criteria and with the SCF convergence set to 10^{-6}.

For the geometry optimisations, the small core Stuttgart-Bonn variety relativistic pseudo potentials (RPPs) were employed for the f elements, together with the associated segmented valence basis sets (without g functions).[63,64] For Se the analogous RPP was employed, with valence functions contracted at the TZP level.[65] Dunning's cc-pVDZ basis sets were used for all other elements.

Single-point calculations were performed at the optimised geometries using the segmented all-electron relativistic basis sets with polarisation functions (SARCP) for the f elements,[66,67] Dunning's cc-pVTZ basis sets for Se and cc-pVDZ for all other elements.[68] Point charge nuclei were used, as recommended for the SARCP basis set, rather than the default Gaussian form. Relativistic effects were included by using the spin–orbit-free Douglas–Kroll–Hess Hamiltonian. The resulting formatted checkpoint files were then used as input to the AIMAll package, version 11,[69] for QTAIM analysis. Cartesian atomic coordinates for all computationally studied complexes are collected in the ESI.†

Acknowledgements

A.J.G. and M.B.J. thank the U.S. Department of Energy, Office of Science, Early Career Research Program (contract DE-AC52-06NA25396) for the experimental aspects of this work. In addition, an initial sample of the uranium complex **8** was prepared under the Heavy Element Chemistry Program, Division of Chemical Sciences, Geosciences, and Biosciences, Office of Basic Energy Sciences, U.S. Department of Energy. N.K. thanks UCL for computing resources *via* the Research Computing "Legion" cluster and associated services.

References

1 *The Chemistry of the Actinide and Transactinide Elements*, ed. L. R. Morss, N. M. Edelstein and J. J. Fuger, Springer, Dordrecht, The Netherlands, 2006.
2 M. B. Jones and A. J. Gaunt, *Chem. Rev.*, in press, DOI: 10.1021/cr300198m.
3 Spent Fuel Reprocessing Options, IAEA-TECDOC-1587, August 2008, http://www-pub.iaea.org/MTCD/publications/PDF/te_1587_web.pdf.
4 G. R. Choppin, *Radiochim. Acta*, 2003, **91**, 645.
5 A. J. Gaunt, S. D. Reilly, A. E. Enriquez, B. L. Scott, J. A. Ibers, P. Sekar, K. I. M. Ingram, N. Kaltsoyannis and M. P. Neu, *Inorg. Chem.*, 2008, **47**, 29.
6 G. R. Choppin, *J. Alloys Compd.*, 2002, **344**, 55.
7 M. P. Jensen and A. H. Bond, *J. Am. Chem. Soc.*, 2002, **124**, 9870.
8 M. Roger, N. Barros, T. Arliguie, P. Thuéry, L. Maron and M. Ephritikhine, *J. Am. Chem. Soc.*, 2006, **128**, 8790.
9 Z. Kolarik, *Chem. Rev.*, 2008, **108**, 4208.
10 C. Ekberg, A. Fermvik, T. Retegan, G. Skarnemark, M. R. S. Foreman, M. J. Hudson, S. Englund and M. Nilsson, *Radiochim. Acta*, 2008, **96**, 225.
11 F. W. Lewis, L. M. Harwood, M. J. Hudson, M. G. B. Drew, J. F. Desreux, G. Vidick, N. Bouslimani, G. Modolo, A. Wilden, M. Sypula, T.-H. Vu and J.-P. Simonin, *J. Am. Chem. Soc.*, 2011, **133**, 13093.
12 Y. Zhu, J. Chen and R. Jiao, *Solvent Extr. Ion Exch.*, 1996, **14**, 61.
13 J. R. Klaehn, D. R. Peterman, M. K. Harrup, R. D. Tillotson, T. A. Luther, J. D. Law and L. M. Daniels, *Inorg. Chim. Acta*, 2008, **361**, 2522.
14 D. R. Peterman, M. R. Greenhalgh, R. D. Tillotson, J. R. Klaehn, M. K. Harrup, T. A. Luther and J. D. Law, *Sep. Sci. Technol.*, 2010, **45**, 1711.
15 M. Mazzanti, R. Wietzke, J. Pécaut, J.-M. Latour, P. Maldivi and M. Remy, *Inorg. Chem.*, 2002, **41**, 2389.
16 J. G. Brennan, S. D. Stults, R. A. Andersen and A. Zalkin, *Organometallics*, 1998, **7**, 1329.
17 L. Karmazin, M. Mazzanti and J. Pécaut, *Chem. Commun.*, 2002, 654.
18 S. G. Minasian, J. L. Krinsky and J. Arnold, *Chem.–Eur. J.*, 2011, **17**, 12234.
19 T. Arliguie, L. Belkhiri, S. E. Bouaoud, P. Thuéry, C. Villiers, A. Boucekkine and M. Ephritikhine, *Inorg. Chem.*, 2009, **48**, 221.
20 D. Guillaumont, *J. Phys. Chem. A*, 2004, **108**, 6893.
21 C. Hill, D. Guillaneux, L. Berthon and C. Madic, *J. Nucl. Sci. Technol.*, 2002, (suppl. 3), 309.
22 K. I. M. Ingram, N. Kaltsoyannis, A. J. Gaunt and M. P. Neu, *J. Alloys Compd.*, 2007, **444–445**, 369.
23 K. I. M. Ingram, M. J. Tassell, A. J. Gaunt and N. Kaltsoyannis, *Inorg. Chem.*, 2008, **47**, 7824.
24 S. Meskaldji, L. Belkhari, T. Arliguie, M. Fourmigue, M. Ephritikhine and A. Boucekkine, *Inorg. Chem.*, 2010, **49**, 3192.
25 M. Miguirditchian, D. Guillaneux, D. Guillaumont, P. Moisy, C. Madic, M. P. Jensen and K. L. Nash, *Inorg. Chem.*, 2005, **44**, 1404.
26 L. Petit, C. Adamo and P. Maldivi, *Inorg. Chem.*, 2006, **45**, 8517.
27 I. Kirker and N. Kaltsoyannis, *Dalton Trans.*, 2011, **40**, 124.
28 I. D. Prodan, G. E. Scuseria and R. L. Martin, *Phys. Rev. B: Condens. Matter Mater. Phys.*, 2007, **76**, 033101.
29 D. D. Schnaars, A. J. Gaunt, T. W. Hayton, M. B. Jones, I. Kirker, N. Kaltsoyannis, I. May, S. D. Reilly, B. L. Scott and G. Wu, *Inorg. Chem.*, 2012, **51**, 8557.
30 M. J. Tassell and N. Kaltsoyannis, *Dalton Trans.*, 2010, **39**, 6719.
31 N. Kaltsoyannis, *Inorg. Chem.*, in press, DOI: 10.1021/ic3006025.
32 R. P. Davies, C. V. Francis, A. P. S. Jurd, M. G. Martinelli, A. J. P. White and D. J. Williams, *Inorg. Chem.*, 2004, **43**, 4802.
33 C. W. Haigh, *Polyhedron*, 1995, **14**, 2871.
34 R. D. Shannon, *Acta Crystallogr., Sect A: Cryst. Phys., Diffr., Theor. Gen. Crystallogr.*, 1976, **32**, 751.
35 A. J. Gaunt, S. D. Reilly, A. E. Enriquez, T. W. Hayton, J. M. Boncella, B. L. Scott and M. P. Neu, *Inorg. Chem.*, 2008, **47**, 8412.
36 A. J. Gaunt and M. P. Neu, *C. R. Chim.*, 2010, **13**, 821.
37 J. N. Cross, E. M. Villa, S. Wang, J. Diwu, M. J. Polinski and T. E. Albrecht-Schmitt, *Inorg. Chem.*, 2012, **51**, 8419.

38 J. Diwu, D. J. Grant, S. Wang, L. Gagliardi and T. E. Albrecht-Schmitt, *Inorg. Chem.*, 2012, **51**, 6906.
39 A. J. Gaunt, B. L. Scott and M. P. Neu, *Inorg. Chem.*, 2006, **45**, 7401.
40 I. May, unpublished work.
41 S. D. Reilly, A. J. Gaunt, B. L. Scott, G. Modolo, M. Iqbal, W. Verboom and M. J. Sarsfield, *Chem. Commun.*, 2012, **48**, 9732.
42 S. D. Reilly, B. L. Scott and A. J. Gaunt, *Inorg. Chem.*, 2012, **51**, 9165.
43 D. Rosario-Amorin, E. N. Duesler, R. T. Paine, B. P. Hay, L. H. Delmau, S. D. Reilly, A. J. Gaunt and B. L. Scott, *Inorg. Chem.*, 2012, **51**, 6667.
44 A. J. Gaunt, I. May, M. P. Neu, S. D. Reilly and B. L. Scott, *Inorg. Chem.*, 2011, **50**, 4244.
45 C. Berthon, N. Boubals, I. A. Charushnikova, D. Collison, S. M. Cornet, C. Den Auwer, A. J. Gaunt, N. Kaltsoyannis, I. May, S. Petit, M. P. Redmond, S. D. Reilly and B. L. Scott, *Inorg. Chem.*, 2010, **49**, 9554.
46 R. F. W. Bader, *Atoms in Molecules: A Quantum Theory*, OUP, Oxford, 1990.
47 V. V. Zhurov, E. A. Zhurova and A. A. Pinkerton, *Inorg. Chem.*, 2011, **50**, 6330.
48 P. L. Arnold, Z. R. Turner, N. Kaltsoyannis, P. Pelekanaki, R. M. Bellabarba and R. P. Tooze, *Chem.–Eur. J.*, 2010, **16**, 9623.
49 S. M. Mansell, N. Kaltsoyannis and P. L. Arnold, *J. Am. Chem. Soc.*, 2011, **133**, 9036.
50 C. F. Matta and R. J. Boyd, in *The quantum theory of atoms in molecules*, ed. C. F. Matta and R. J. Boyd, Wiley-VCH, Weinheim, 2007, pp. 1–34.
51 L. R. Avens, S. G. Bott, D. L. Clark, A. P. Sattelberger, J. G. Watkin and B. D. Zwick, *Inorg. Chem.*, 1994, **33**, 2248.
52 S. G. Minasian, K. S. Boland, R. K. Feller, A. J. Gaunt, S. A. Kozimor, I. May, S. D. Reilly, B. L. Scott and D. K. Shuh, *Inorg. Chem.*, 2012, **51**, 5728.
53 *APEX II 1.08*, Bruker AXS, Inc., Madison, Wisconsin 53719, 2004.
54 *SAINT+ 7.06*, Bruker AXS, Inc., Madison, Wisconsin 53719, 2003.
55 G. Sheldrick, *SADABS 2.03*, University of Göttingen, Germany, 2001.
56 *SHELXTL 5.10*, Bruker AXS, Inc., Madison, Wisconsin 53719, 1997.
57 A. L. Spek, *J. Appl. Crystallogr.*, 2003, **36**, 7.
58 *SMART 4.210*, Bruker AXS, Inc., Madison, Wisconsin 53719, 1996.
59 *SAINT 5.050*, Bruker AXS, Inc., Madison, Wisconsin 53719, 1998.
60 *SHELXTL 6.10*, Bruker AXS, Inc., Madison, Wisconsin 53719, 2001.
61 C. Adamo and V. Barone, *J. Chem. Phys*, 1999, **110**, 6158.
62 M. J. Frisch, G. W. Trucks, H. B. Schlegel, G. E. Scuseria, M. A. Robb, J. R. Cheeseman, G. Scalmani, V. Barone, B. Mennucci, G. A. Petersson, H. Nakatsuji, M. Caricato, X. Li, H. P. Hratchian, A. F. Izmaylov, J. Bloino, G. Zheng, J. L. Sonnenberg, M. Hada, M. Ehara, K. Toyota, R. Fukuda, J. Hasegawa, M. Ishida, T. Nakajima, Y. Honda, O. Kitao, H. Nakai, T. Vreven, J. A. Montgomery, J. E. Peralta, F. Ogliaro, M. Bearpark, J. J. Heyd, E. Brothers, K. N. Kudin, V. N. Staroverov, R. Kobayashi, J. Normand, K. Raghavachari, A. Rendell, J. C. Burant, S. S. Iyengar, J. Tomasi, M. Cossi, M. Rega, N. J. Millam, M. Klene, J. E. Knox, J. B. Cross, V. Bakken, C. Adamo, J. Jaramillo, R. E. Gomperts, O. Stratmann, A. J. Yazyev, R. Austin, C. Cammi, J. W. Pomelli, R. Ochterski, R. L. Martin, K. Morokuma, V. G. Zakrzewski, G. A. Voth, P. Salvador, J. J. Dannenberg, S. Dapprich, A. D. Daniels, O. Farkas, J. B. Foresman, J. V. Ortiz, J. Cioslowski and D. J. Fox, Gaussian,Inc., Wallingford CT, 2009.
63 X. Y. Cao and M. Dolg, *J. Mol. Struct.: THEOCHEM*, 2002, **581**, 139.
64 X. Y. Cao and M. Dolg, *J. Mol. Struct.: THEOCHEM*, 2004, **673**, 203.
65 J. M. L. Martin and A. Sundermann, *J. Chem. Phys.*, 2001, **114**, 3408.
66 D. A. Pantazis and F. Neese, *J. Chem. Theory Comput.*, 2009, **5**, 2229.
67 D. A. Pantazis and F. Neese, *J. Chem. Theory Comput.*, 2011, **7**, 677.
68 E. R. Davidson, *Chem. Phys. Lett.*, 1996, **260**, 514.
69 T. A. Keith, *TK Gristmill Software*, 11.10.16 edn, 2011.